

# Imaging cellular network dynamics in three dimensions using fast 3D laser scanning

Werner Göbel, Björn M Kampa & Fritjof Helmchen

**Spatiotemporal activity patterns in three-dimensionally organized cellular networks are fundamental to the function of the nervous system. Despite advances in functional imaging of cell populations, a method to resolve local network activity in three dimensions has been lacking. Here we introduce a three-dimensional (3D) line-scan technology for two-photon microscopy that permits fast fluorescence measurements from several hundred cells distributed in 3D space. We combined sinusoidal vibration of the microscope objective at 10 Hz with 'smart' movements of galvanometric x-y scanners to repeatedly scan the laser focus along a closed 3D trajectory. More than 90% of cell somata were sampled by the scan line within volumes of 250  $\mu\text{m}$  side length. Using bulk-loading of calcium indicator, we applied this method to reveal spatiotemporal activity patterns in neuronal and astrocytic networks in the rat neocortex *in vivo*. Two-photon population imaging using 3D scanning opens the field for comprehensive studies of local network dynamics in intact tissue.**

Proper functioning of any organ relies on the coordinated activity of its cellular constituents, which typically are organized in 3D networks. Network dynamics is particularly important in the brain where highly interconnected populations of neurons and glial cells form excitable circuits that subservise sensory processing, memory formation and generation of motor commands. However, experimental methods to directly measure local network activity in the intact brain have been limited. Intracellular *in vivo* recordings have been obtained from pairs of cells at most<sup>1</sup>. Extracellular multielectrode recordings permit simultaneous recordings from hundreds of neurons<sup>2</sup>, but samples are taken from widely distributed populations with poorly defined cell types and spatial relationships. Alternatively, optical microscopy allows functional imaging of local network dynamics with cellular resolution. Recent advances in two-photon-excited fluorescence laser-scanning microscopy (2PLSM)<sup>3–5</sup> and new population-staining methods<sup>6,7</sup> now permit *in vivo* measurements of spatiotemporal activity patterns in neuronal and glial networks<sup>6–10</sup>. Although 3D maps of activity can be built up for reproducible stimuli using sequential measurements at different focal depths<sup>11,12</sup>, single-trial imaging so far has been restricted to

two dimensions with rather arbitrary subsets of cells in the local 3D network sampled.

Extending population measurements to three dimensions is difficult because scanning technology usually necessitates a compromise between temporal resolution and the size of the measured area or volume. On long time scales (minutes to days) the acquisition of time series of image stacks is sufficient to study morphological plasticity<sup>13</sup>. Depending on the number of planes, the temporal resolution of such four-dimensional time-lapse imaging<sup>14</sup> is typically limited to less than 0.1 Hz because stepwise focal-plane changes are slow. Using continuous movement of the microscope objective, acquisition rates of 0.4 Hz could be achieved<sup>15</sup>. To resolve neuronal activity patterns, however, a higher temporal resolution is required. For example, spike-pattern detection based on action potential-evoked calcium transients requires acquisition rates of  $\geq 10$  Hz because somatic calcium transients typically decay with a time constant of a few hundred milliseconds<sup>10</sup>.

How can one achieve sufficiently fast volume imaging of large numbers of cells? The key technology is to provide fast scanning along the optical axis. Such z-dimension scanning has been implemented using various devices, including piezoelectric focusing elements<sup>16</sup>, variable-focus lenses<sup>17</sup>, deformable mirrors<sup>18</sup> and special arrangements of acousto-optical deflectors (AODs)<sup>19</sup>. None of these approaches has led to 3D network imaging yet. Here we present a 3D imaging approach based on piezoelectrically induced mechanical vibration of the microscope objective. The basic idea is to perform a 3D line-scan that passes through as many cell bodies as possible. Our approach is simple, uses commercially available components and is generally applicable. We demonstrate *in vivo* calcium imaging from several hundred cells with 10-Hz temporal resolution, and visualize 3D population activity in local networks of neurons and astrocytes in the neocortex.

## RESULTS

### 3D laser scanning

The principal idea for rapid volume scanning is to create a 3D trajectory that is repeatedly scanned by the laser focus and optimized for sampling as many cell bodies as possible. We implemented 3D line-scanning in a custom-built 2PLSM using

Department of Neurophysiology, Brain Research Institute, University of Zurich, Winterthurerstr. 190, CH-8057 Zürich, Switzerland. Correspondence should be addressed to F.H. (helmchen@hifo.unizh.ch).

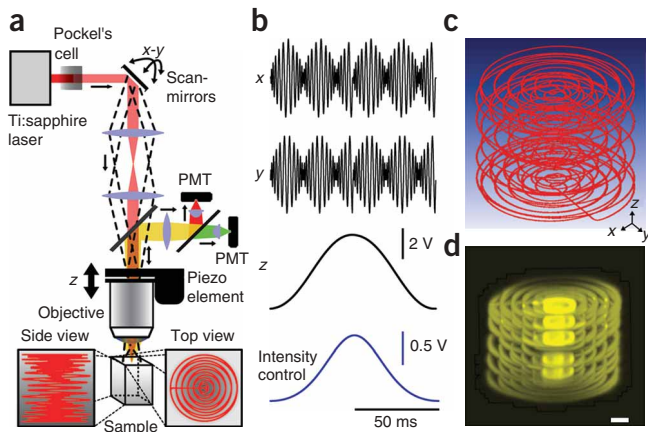


**Figure 1** | Principle of 3D laser scanning. (a) Two-photon microscope setup for 3D line-scanning. Galvanometric scan mirrors were used for  $x$ - $y$  scanning. A piezoelectric focusing element induced sinusoidal vibration of the objective along the optical axis ( $z$  axis). (b) Lateral  $x$ - $y$  position signals (top) during one cycle of the objective's  $z$ -motion (middle). In this example 10-Hz vibration and a spiral pattern in the  $x$ - $y$  plane were used. For automatic intensity adjustment, light transmission through the Pockel's cell was modulated during each cycle according to focal depth (bottom). (c) Reconstruction of the 3D scan trajectory corresponding to the position signals in b. (d) Direct visualization of a 3D scan pattern by integrating video images of the trajectory of a two-photon-excited fluorescence spot in a fluorescein solution ( $10\times$  objective). Scale bar,  $50\ \mu\text{m}$ .

two standard galvanometric scan mirrors for  $x$ - $y$  scanning and a piezoelectric focusing element for  $z$  scanning (Fig. 1a). Driving the piezo element with a sinusoidal voltage induced mechanical vibration of the microscope objective along the optical axis (Fig. 1b). At 10 Hz and using a  $40\times$  water immersion objective, we were able to achieve amplitudes of  $200$ – $300\ \mu\text{m}$  easily. Depending on the frequency and the load (that is, the objective type) adjustments of the drive signals were necessary to compensate for amplitude reduction and phase shift (see **Supplementary Methods** online; full frequency curves are available in **Supplementary Fig. 1** online).

Matched to the sinusoidal movement of the objective, we calculated appropriate driving signals for the  $x$ - $y$  scanners to create a 3D trajectory. In the simplest case, we used a spiral pattern in the  $x$ - $y$  plane (Fig. 1b,c). To directly relate 3D-line-scan data to a previously acquired reference image stack, we always reconstructed the actual scan pattern from the position feedback signals provided by the galvanometers and the piezo element. The line generation algorithm ensured that scan points were equidistant in 3D space and that the pixel dwell time was constant for the entire scan line (typically  $10\ \mu\text{s}$ ; see **Supplementary Methods**). As a result, lateral steps in the  $x$ - $y$  plane had to be largest at the upper and lower limits of the sinusoidal vibration where the velocity of the microscope objective is smallest. The 3D-line-scan pattern was directly visualized by video imaging (Fig. 1d and **Supplementary Video 1** online).

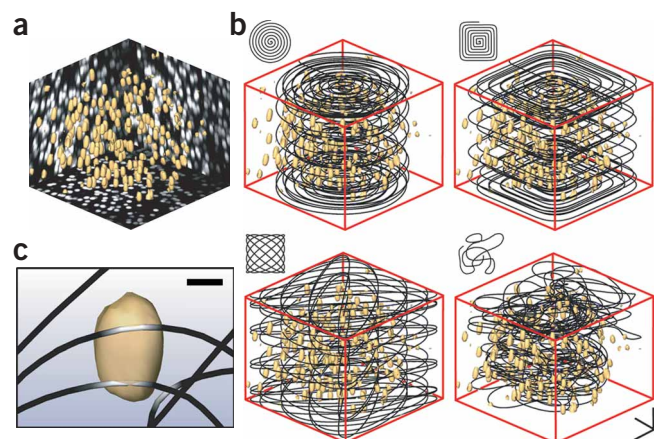
Light scattering in biological tissue reduces two-photon excitation with focal depth<sup>20,21</sup>. Depending on the scattering properties of the sample, we therefore compensated excitation loss during 3D laser scanning by automatically adjusting the average laser power according to the focal depth using a Pockel's cell (Fig. 1b and **Supplementary Methods**). For neocortical tissue we assumed an exponential decrease with a scattering length of  $200$ – $250\ \mu\text{m}$ <sup>20,21</sup>.

**Figure 2** | Alternative modes for 3D laser scanning. (a) Reference image stack of  $10\text{-}\mu\text{m}$  fluorescent beads embedded in agar. Single beads are shown in isosurface view (yellow). Additionally, maximum intensity projections of  $x$ - $y$ ,  $x$ - $z$  and  $y$ - $z$  planes are shown. (b) Visualization of spiral (top left), square-spiral (top right), Lissajous (bottom left) and user-defined (bottom right) 3D scan patterns applied to the volume shown in a. Pixel dwell time and 3D spacing of scan points were the same for all modes (referring only to relevant segments in user-defined mode). Scale bars,  $50\ \mu\text{m}$ . (c) Close-up view of a single bead and segments of the scan trajectory. Fluorescence intensities along the scan line were encoded by gray values. Fluorescence increases were consistent with bead position. Scale bar,  $5\ \mu\text{m}$ .

### 3D scanning modes

Our goal was to permit measurements from cell bodies distributed in 3D space. We therefore implemented various modes of 3D laser scanning and tested their volume scanning properties (Fig. 2). First, we used different analytical functions for  $x$ - $y$  scanning, resulting in spiral, square-spiral or Lissajous patterns, respectively (Fig. 2b and **Supplementary Methods**). Scan density and the number of  $x$ - $y$  scan-pattern repeats per sinus period of the objective's motion were chosen to optimize volume coverage. A  $180^\circ$ -phase jump in the  $x$  and  $y$  command signals at upper and lower  $z$ -limits ensured that the maxima of lateral scanning were interleaved for downward and upward movement of the objective (Fig. 1b). As a second alternative method, we devised a user-defined 3D scanning mode (Fig. 2b). In this mode multiple points of interest (for example, fluorescent beads or cell somata) were selected from the previously acquired reference stack. After appropriate sorting of the selected points, a smooth and continuous 3D scan line passing through all points was calculated (**Supplementary Fig. 2** online). In contrast to the analytical modes, which used constant pixel dwell time and 3D pixel distance along the entire scan trajectory, the user-defined approach generally required piecewise scanning of the trajectory with intermittent segments of decreased or increased velocity (**Supplementary Fig. 3** online).

We evaluated the stability of 3D laser scanning using  $10\text{-}\mu\text{m}$  fluorescent beads embedded in agarose (Fig. 2a). We chose the density of the beads ( $32,000 \pm 2,000\ \text{beads}/\text{mm}^3$ ;  $n = 3$ ; mean  $\pm$  s.d.) to be in the range of cell densities in the rat neocortex. Using a  $40\times$  water-immersion objective, we acquired 3D line-scans at 10-Hz repetition rate within volumes of  $200$ – $300\ \mu\text{m}$  side length. Comparison of 3D-line-scan fluorescence signals with the



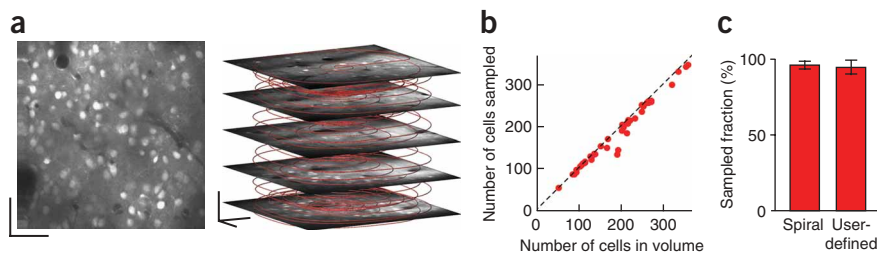


**Figure 3** | Sampling of cell populations by 3D laser scanning. **(a)** *In vivo* two-photon fluorescence image of cells in layer 2 of rat somatosensory cortex stained by bolus loading with the calcium indicator OGB-1 AM (left). A 3D view showing five example image planes of a reference image stack overlaid by a spiral 3D scan trajectory (right). Scale bars, 50  $\mu\text{m}$ . **(b)** Number of cell somata sampled by the 3D scan trajectory versus total number of somata in the volume covered. Pooled data from several spiral mode experiments for tissue cubes of different volume. **(c)** Summary plot of the mean sampling fraction (mean  $\pm$  s.d.;  $n = 34$  and 8 for spiral and user-defined mode, respectively) for cell somata in superficial neocortical layers using spiral and user-defined mode.

respective reference stack showed that high-intensity values were obtained exactly at the positions of the beads (**Fig. 2c**). Individual beads could be hit several times by the scan line. For several minutes of continuous recording the intensity distribution of individual bead pixel showed a noise level comparable to that for conventional raster-scanning, demonstrating that the 3D line-scan was reliably repeated over time (**Supplementary Fig. 4** online).

We next analyzed volume coverage of the different modes. First, we subdivided the scanned volume ( $0.25 \times 0.25 \times 0.2$  mm) into cubes of variable side length and analyzed the fraction of cubes traversed by the scan line. In spiral, square-spiral and Lissajous mode, this fraction was about 50% and 90% for 15- $\mu\text{m}$  and 30- $\mu\text{m}$  cubes, respectively. In user-defined mode, the fraction was consistently smaller (40% and 80%). Second, we evaluated the fraction of fluorescent beads hit by the 3D line-scan. For spiral and square-

spiral mode this fraction was  $71 \pm 3.5\%$  and  $69 \pm 3\%$ , respectively ( $n = 3$ ). Fewer beads ( $44 \pm 1.5\%$ ) were sampled in Lissajous mode, which covered the volume less homogeneously. Not surprisingly, user-defined 3D line-scanning sampled the highest percentage of beads ( $92 \pm 3.5\%$ ) at the lowest volume coverage. Because spiral and user-defined modes were best suited for object sampling, we further evaluated them for 3D measurements of cell populations.

We loaded the acetoxymethyl (AM) ester form of the calcium indicator dye Oregon Green BAPTA-1 (OGB-1 AM) into cells in the neocortex of anesthetized rats using the multicell bolus loading technique<sup>6</sup> (**Fig. 3a**). We acquired 3D line-scans from volumes of variable size (up to 250  $\mu\text{m}$  side length)

containing up to several hundred cells and analyzed the fraction of cells that were sampled ('hit') by the trajectory within the total volume (for spiral mode a cylindrical volume was considered). High-sampling fractions of more than 90% could be achieved with both spiral and user-defined mode (**Fig. 3b,c**). The higher fraction of sampled cells compared to the bead measurements is explained by the larger diameter of cell bodies. In practice, a disadvantage of the user-defined mode currently is the time-consuming procedure of cell selection. We therefore applied the spiral or square-spiral mode of 3D scanning to obtain functional measurements of spatiotemporal activity patterns from cellular networks *in vivo*.

### 3D calcium imaging of neuronal- and glial-network dynamics

Bolus loading of calcium indicator results in unspecific staining of cells within a volume with a diameter of several hundred

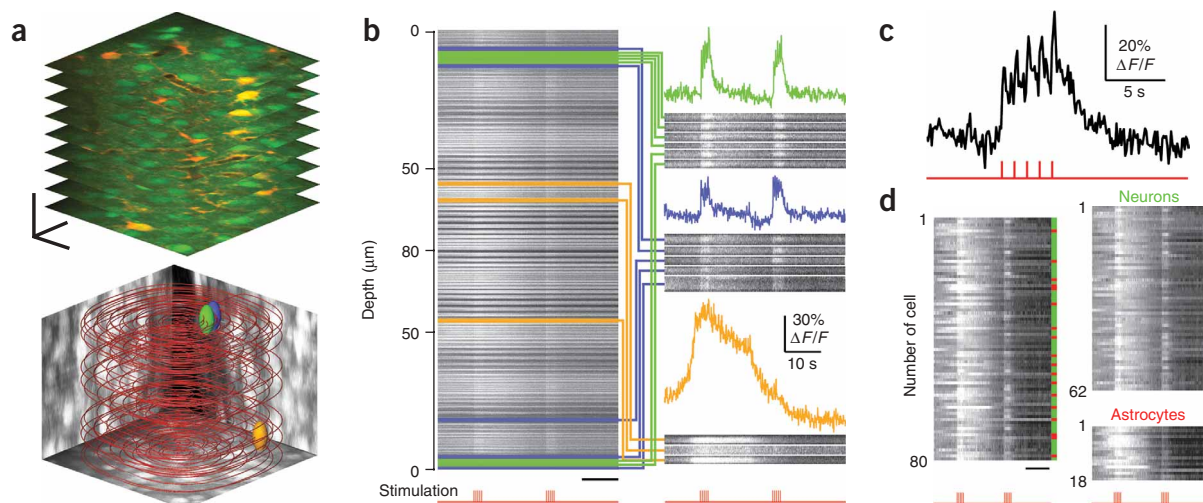


**Figure 4** | Signal assignment to cells. **(a)** Reference image stack from neocortical layer 2 (top). Cells were stained with calcium indicator (green) and the astrocyte-specific SR101 (red). Dual-stained astrocytes appear yellow. Scale bars, 25  $\mu\text{m}$ . Applied spiral 3D scan trajectory (bottom). Three ellipsoids (green, blue and yellow) are shown representing the positions and VOIs of three example cell somata selected from the reference stack. **(b)** Entire set of line-scan raw data (left). Line-scan segments within the VOIs selected in **a** were assigned to the corresponding cells (same color code as in **a**; right). For each cell fluorescence signals of all sections were averaged revealing the time course of the calcium signal. Stimulation through an extracellular micropipette consisted of several series of 5 bursts of 10 pulses at 100 Hz (1-s burst interval). Scale bar, 10 s. **(c)** Enlarged view of neuronal calcium transients evoked in the green cell by five bursts of 100-Hz pulses. **(d)** Complete set of cellular calcium signals analyzed as exemplified for the three cells in **a** and **b** (left). The bar on the right indicates the identification of cells using SR101 as neurons (green) or astrocytes (red). Separated plots of calcium signals in neurons and astrocytes (right). Scale bar, 10 s.

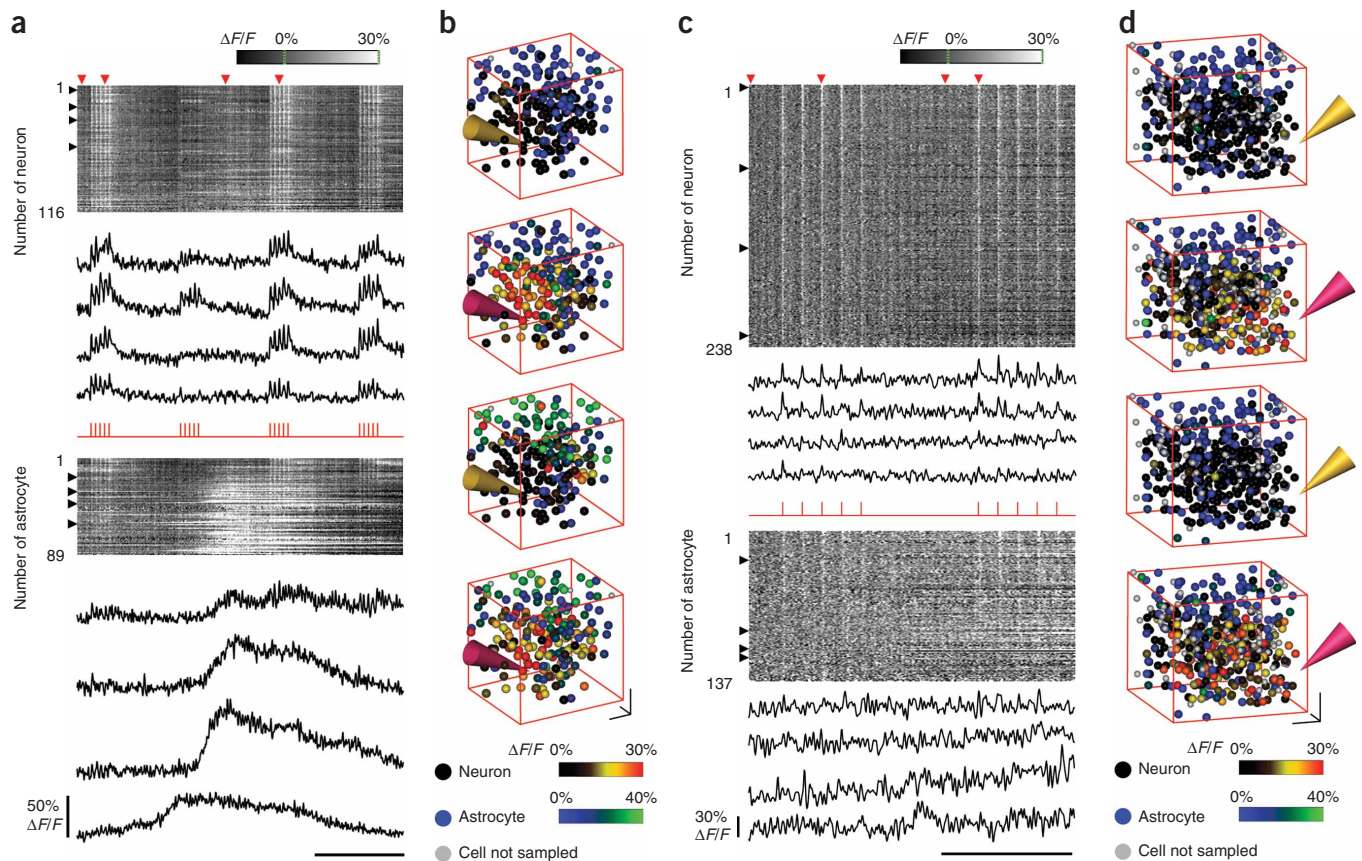


**Figure 5** | Visualization of spatiotemporal calcium dynamics in large neuronal and glial cell populations. **(a)** Neuronal (top) and astrocytic (bottom) fluorescence signals at the border of neocortical layer 1 and 2 (205 of 208 total cells sampled by 10-Hz spiral 3D scanning). Cells were sorted according to their 3D distance from the stimulation pipette. For both neurons and astrocytes four example traces are shown for the cells marked by black arrowheads. Stimulation consisted of several series of five bursts of ten current pulses at 100 Hz (1-s burst interval; red trace). Scale bar, 20 s. **(b)** Reconstructed 3D calcium dynamics in the cell populations shown in **a**. Different lookup tables were used for neurons and astrocytes. Calcium signal snapshots are from the four time points indicated by red arrowheads (from top to bottom). Note the neuronal responses induced by electrical stimulation and the calcium wave in layer 1. The stimulation pipette is schematically outlined (yellow: no stimulation; red: stimulation). Scale bars, 50  $\mu$ m. **(c)** Similar data from a different rat from the border layer 1/layer 2 with a sparse stimulation protocol (375 of 458 total cells sampled by 10-Hz spiral 3D scanning). Stimulation consisted of individual pulses (100  $\mu$ s; 5 mA) delivered at 3-s intervals (red trace). Scale bar, 20 s. **(d)** 3D reconstruction of calcium dynamics in the cell population shown in **c**. Snapshots are from the four time points indicated by red arrowheads. Scale bars, 50  $\mu$ m.

micrometers<sup>6</sup>. To discriminate neuronal and glial subpopulations, we additionally applied the red fluorescent dye sulforhodamine 101 (SR101), which specifically stains astrocytes<sup>7</sup> (Fig. 4a). For each experiment, we acquired a reference image stack, from which 3D coordinates of cell bodies were determined and related to the 3D scan trajectory (Fig. 4a). We performed volume scanning at 10 Hz with a 40 $\times$  water-immersion objective while cells were stimulated with current pulses through an extracellular micropipette positioned nearby.

A critical issue in our data analysis was to correctly assign fluorescence signals to the individual cells. Because cells often were hit multiple times by different segments of the scan trajectory, the signal-to-noise ratio could be improved by averaging all signal components from a particular cell. To this end, we defined ellipsoid ‘volumes of interest’ (VOIs) that enclosed the somata of identified cells based on the reference image stack (Fig. 4a). All segments of the 3D scan line within each VOI were ‘cut out’ and the respective calcium signals were averaged (Fig. 4b). We expressed fluorescence signals as relative fluorescence changes ( $\Delta F/F$ ) using the minimum

fluorescence (usually from inside a blood vessel) as fluorescence background. In Figure 4b this approach is exemplified for three cells in a rather small volume (80 cells in total). Two of the cells were identified as neurons that were hit 5 and 6 times, respectively. In response to repetitive electrical stimulation these neurons displayed summation of rapid calcium transients, which presumably were evoked by action potentials (Fig. 4c). The third example cell was an astrocyte that was hit three times and showed a much slower transient increase in calcium concentration. Based on the SR101 counterstain, two separate plots of the time course of the calcium signal for all sampled cells were obtained for astrocytic and neuronal subpopulations (Fig. 4d).

Finally, we aimed to visualize 3D calcium dynamics within the sampled volume. Figure 5a shows another example of simultaneous calcium imaging from neurons and astrocytes in a larger volume. Most neurons responded reliably to extracellularly applied stimuli. Note that a large, long-lasting wave of calcium elevation spread throughout the astrocytic network (Fig. 5a). Using the 3D visualization software Amira, we schematically represented all cells

at their 3D positions using colored spheres. To each cell (sphere) we then assigned the entire, color-coded time course of the respective fluorescence signal (Fig. 5b). Using this approach, the spatiotemporal activity pattern could be visualized simultaneously in the neuronal and glial network. The 3D visualization software permitted inspection of the dynamic patterns from all sides and angles (see **Supplementary Video 2** online). Similar data were obtained in six experiments using electrical stimulation. In several cases we also used minimal stimulation by delivering trains of single pulses (Fig. 5c,d and **Supplementary Video 3** online). Although the signal-to-noise ratio was reduced, we could clearly resolve neuronal calcium transients that occurred in an all-or-none manner depending on stimulation intensity. This finding suggests that the sensitivity of our fluorescence measurements is close to single-spike resolution, which, however, needs to be confirmed by using simultaneous electrophysiological recordings<sup>10</sup>.

In another series of experiments we locally injected the GABA<sub>A</sub> receptor antagonist bicuculline (2 mM) through a micropipette ( $n = 3$ ). This protocol elicited long-lasting spontaneous activity in superficial neocortical cell populations. Large coordinated calcium signals occurred in the neuronal population and in some of the glial cells that were synchronized to seizure-like peaks in the simultaneously recorded local field potential (**Supplementary Video 4** online).

## DISCUSSION

The common model of brain function presumes that sensory stimuli, internal brain states, as well as motor commands are represented in the activity patterns of neuronal networks. Most neural processing occurs in local microcircuits (containing on the order of several hundred neurons) with long-range interconnecting transmission lines. The study of local network dynamics thus is fundamental to neuroscience but requires simultaneous recordings of large cell populations in the intact brain. Here we introduced a new laser-scanning technique that allows *in vivo* calcium imaging from hundreds of cells in volumes of up to 250  $\mu\text{m}$  side length. This method for the first time permits functional imaging in three dimensions, with sufficiently high temporal resolution (10 Hz) to resolve neuronal responses and reconstruct local network activity.

Spatiotemporal activation patterns in cells or cell populations have been measured previously using different imaging techniques. For example, fast camera systems permit calcium imaging from large cell populations<sup>22</sup>. Alternatively, multisite recordings are achieved using various laser-scanning approaches, including resonant galvanometers<sup>16</sup>, confocal spinning disks<sup>23,24</sup>, AODs<sup>25,26</sup> or multifocal-beam scanning<sup>27</sup>. All these methods are limited in so far as they sample from locations that lie within a two-dimensional (2D) plane. Owing to the intrinsic 3D organization of most cellular networks, it is essential to expand the range of optical recordings to three dimensions by using fast *z*-dimension scanning<sup>16–18</sup>. Recently, a scheme for fast 3D laser scanning using AODs has been proposed<sup>19</sup>, which is, however, technically demanding and currently limited in terms of optical aberrations and applicability to 2PLSM. Alternatively, swinging of the microscope objective along the optical axis has been used for fast *x-z* imaging<sup>16</sup>. Here we extended this method to three dimensions by implementing a full 3D line-scan. In contrast to standard 2D line-scans, which aim at highest temporal resolution, the goal was here to use a 3D scan trajectory for extensive volume

scanning at acquisition rates comparable to typical frame rates of 2D imaging systems.

The major advantages of our approach are simplicity, lack of power losses and optical aberrations, and the commercial availability of all components. It should be noted, however, that—owing to the use of mechanical components—deviations from the desired scan trajectory occur. In our experiments the mean deviation of the actual from the desired trajectory typically was 1–3  $\mu\text{m}$ , mainly owing to a small departure of the *z*-motion from sinusoidal shape. These deviations were tolerable in our experiments because we always used the feedback position signals to reconstruct the actual scan trajectory and assign fluorescence signals to the cells. Only for the user-defined mode, where specific locations are targeted, it will be important to further improve scan accuracy, for example, using predictive scan electronics. Additionally, automatic cell detection in the 3D reference stack should reduce the time for finding cell coordinates. Different from 2D imaging, individual cells are sampled in the 3D modes by line segments that contain only a few pixels (typically 2–3 pixels for volumes of 250- $\mu\text{m}$  side length; pixel size 4  $\mu\text{m}$  for 10- $\mu\text{s}$  dwell time). Sparse sampling may reduce the signal-to-noise ratio, but this problem is alleviated because most cells are usually hit several times (on average  $2.1 \pm 0.6$  times;  $n = 580$  cells), so that multiple scan segments can be combined (Fig. 4).

Three-dimensional laser scanning is particularly well suited to reveal local activity patterns in cellular networks. Compared to multisite extracellular recordings, which sample widely dispersed neuronal populations at high temporal resolution<sup>2</sup>, 3D laser scanning has complementary features, permitting nearly complete measurements of local network dynamics with well-defined cell identities and locations. Additionally, neuronal and glial cell activities can be monitored simultaneously, permitting further studies on neuron-glial interactions and the potential role of glial cells in sensory processing<sup>28</sup>. Further discrimination of cell types may be achieved using transgenic animals with cell-specific expression of fluorescent proteins<sup>29</sup>. Using OGB-1, we recently demonstrated that two-photon calcium imaging achieves single-spike sensitivity<sup>10</sup>. Moreover, instantaneous spike rates can be reconstructed even at high firing rates<sup>12</sup>. Here we detected small calcium transients in response to individual extracellular stimuli, presumably reflecting single or a few spikes, but it remains a challenge to establish single-spike detection in the entire volume sampled. In the future, ion concentrations and other physiological variables, such as membrane potential, neurotransmitter release or enzyme activity, might be directly read out by genetically encoded functional indicators<sup>30</sup>.

In summary, the novel 3D laser scanning technique opens the field for comprehensive studies of local cellular network dynamics. The method can be broadly applied to any type of tissue, in which the coordinated activity of three-dimensionally organized cell networks is essential. For neuroscientists 3D laser scanning provides a new means to reveal principles of neural processing on the level of microcircuits, for example, within a cortical column, and thus is most promising to bridge the gap between large-scale and high-resolution functional imaging.

## METHODS

**Two-photon microscopy and 3D laser scanning.** We used a custom built 2PLSM with 100-fs laser pulses at 870-nm wavelength

provided by a Ti:sapphire laser system (Spectra-Physics). We modulated laser intensity using a Pockel's cell (Conoptics). We adjusted beam size with a telescope. We used two galvanometric scan mirrors (model 6210; Cambridge Technology) for  $x$ - $y$  scanning. For rapid  $z$ -dimension scanning along the optical axis we used a piezoelectric focusing element with up to 400  $\mu\text{m}$  travel in closed-loop mode (P-725.4CD PIFOC, E-665 control electronics; Physik Instrumente). We acquired fluorescence data through a water-immersion objective (40 $\times$  LUMPlanFl/IR; 0.8 numerical aperture (NA); Olympus) using laser-scanning software custom-written in the LabView environment (National Instruments). Special routines for 3D scanning were also custom-written in LabView (**Supplementary Software** online). We sampled photomultiplier signals at 10 MHz and digitally integrated them over pixel dwell times.

**Rat preparation and fluorescence labeling.** All animal procedures were carried out according to the guidelines of the Center for Laboratory Animals of the University of Zurich, and were approved by the Cantonal Veterinary Office. We anesthetized Wistar rats (16–28 days old) with urethane (1.5 g/kg of body weight) and made a craniotomy above the somatosensory cortex, as described previously<sup>7,10</sup>. We carefully removed the dura and superfused the exposed cortex with normal rat Ringer (NRR) solution (135 mM NaCl, 5.4 mM KCl, 5 mM Hepes, 1.8 mM CaCl<sub>2</sub>; pH to 7.2 with NaOH). To dampen heartbeat- and breathing-induced motion, we filled the cranial window with agarose (type III-A, Sigma; 1% in NRR) and covered it with an immobilized glass coverslip.

We labeled cell populations in superficial neocortical layers with a calcium indicator using the multicell bolus loading technique<sup>6</sup>. Briefly, we dissolved 50  $\mu\text{g}$  of OGB-1 AM (Molecular Probes) in DMSO plus 20% Pluronic F-127 (BASF) and diluted this solution in NRR to a final concentration of 1 mM. We then pressure-ejected this solution into neocortical layer 2/3 using a micropipette<sup>10</sup>. Brief application of SR101 to the exposed neocortical surface resulted in colabeling of the astrocytic network<sup>7</sup>. For electrical stimulation, we delivered current pulses (100- $\mu\text{s}$ ; 0.1–5 mA) through a glass electrode ( $\sim 2$ - $\mu\text{m}$  tip size) placed near to or within the imaging volume. We included Alexa 594 (20  $\mu\text{M}$ ) in the electrode solution for visualization.

**Data analysis.** From the reference image stack, we identified by hand the 3D coordinates of all cell somata. Centered on the cells, we defined ellipsoid VOIs with  $z$  diameters twice as large as the  $x$ - $y$  diameters. We chose elongated VOIs along the  $z$  direction to better fit the shape of cell-somata images, consistent with the poorer microscope resolution in the  $z$  direction. We then compared VOIs to the coordinates of the 3D scan trajectory and identified all line-scan segments within a particular VOI. We averaged fluorescence signals from all pixels inside a VOI and expressed the calcium signals as relative fluorescence changes ( $\Delta F/F$ ) after subtraction of a background, which was determined as the minimum of the mean of all 3D scan points over time (typically from inside a blood vessel lumen). Analysis routines were custom-written in LabView (National Instruments). We visualized scan trajectories as well as network calcium dynamics using the 3D visualization software Amira (Mercury Computer Systems). We generated time series of 3D population activity by

assigning cellular fluorescence signals to color-coded spheres using a PSI file format.

**Additional methods.** In **Supplementary Methods**, we provide a detailed description of the algorithms for generating 3D trajectories in the different scanning modes and of the automatic adjustment of laser intensity with imaging depth.

*Note: Supplementary information is available on the Nature Methods website.*

#### ACKNOWLEDGMENTS

We thank J.N.D. Kerr for help with initial experiments, J. Waters for help with LabView programming, H.J. Kasper, J. Tritthardt and S. Giger for excellent technical support, and R.W. Friedrich, J.N.D. Kerr and K.A. Martin for comments on the manuscript. This work was supported by a Human Frontier Science Program research grant to F.H. (RGP0009/2004-C) and a predoctoral fellowship of the Neuroscience Center Zurich to W.G.

#### AUTHOR CONTRIBUTIONS

W.G. and F.H. devised the method and designed the microscope system; W.G. wrote the software; W.G. and B.M.K. performed the experiments; W.G., B.M.K. and F.H. jointly wrote the manuscript.

#### COMPETING INTERESTS STATEMENT

The authors declare competing financial interests (see the *Nature Methods* website for details).

Published online at <http://www.nature.com/naturemethods/>  
Reprints and permissions information is available online at  
<http://npg.nature.com/reprintsandpermissions/>

- Lampl, I., Reichova, I. & Ferster, D. Synchronous membrane potential fluctuations in neurons of the cat visual cortex. *Neuron* **22**, 361–374 (1999).
- Buzsaki, G. Large-scale recording of neuronal ensembles. *Nat. Neurosci.* **7**, 446–451 (2004).
- Denk, W., Strickler, J.H. & Webb, W.W. Two-photon laser scanning fluorescence microscopy. *Science* **248**, 73–76 (1990).
- Helmchen, F. & Denk, W. Deep tissue two-photon microscopy. *Nat. Methods* **2**, 932–940 (2005).
- Tsai, P.S. *et al.* Principles, design, and construction of a two photon laser scanning microscope for *in vitro* and *in vivo* brain imaging. In *In Vivo Optical Imaging of Brain Function* (ed., Frostig, R.D.) 113–171 (CRC Press, Boca Raton, 2002).
- Stosiek, C., Garaschuk, O., Holthoff, K. & Konnerth, A. *In vivo* two-photon calcium imaging of neuronal networks. *Proc. Natl. Acad. Sci. USA* **100**, 7319–7324 (2003).
- Nimmerjahn, A., Kirchhoff, F., Kerr, J.N.D. & Helmchen, F. Sulforhodamine 101 as a specific marker of astroglia in the neocortex *in vivo*. *Nat. Methods* **1**, 31–37 (2004).
- Hirase, H., Qian, L., Bartho, P. & Buzsaki, G. Calcium dynamics of cortical astrocytic networks *in vivo*. *PLoS Biol.* **2**, E96 (2004).
- Ohki, K., Chung, S., Ch'ng, Y., Kara, P. & Reid, R. Functional imaging with cellular resolution reveals precise micro-architecture in visual cortex. *Nature* **433**, 597–603 (2005).
- Kerr, J.N.D., Greenberg, D. & Helmchen, F. Imaging input and output of neocortical networks *in vivo*. *Proc. Natl. Acad. Sci. USA* **102**, 14063–14068 (2005).
- Ohki, K. *et al.* Highly ordered arrangement of single neurons in orientation pinwheels. *Nature* **442**, 925–928 (2006).
- Yaksi, E. & Friedrich, R.W. Reconstruction of firing rate changes across neuronal populations by temporally deconvolved Ca<sup>2+</sup> imaging. *Nat. Methods* **3**, 377–383 (2006).
- Majewska, A.K. & Sur, M. Plasticity and specificity of cortical processing networks. *Trends Neurosci.* **29**, 323–329 (2006).
- Gerlich, D. & Ellenberg, J. 4D imaging to assay complex dynamics in live specimens. *Nat. Cell Biol. (Suppl.)*, S14–S19 (2003).
- Hammond, A.T. & Glick, B.S. Raising the speed limits for 4D fluorescence microscopy. *Traffic* **1**, 935–940 (2000).
- Callamaras, N. & Parker, I. Construction of a confocal microscope for real-time  $x$ - $y$  and  $x$ - $z$  imaging. *Cell Calcium* **26**, 271–279 (1999).
- Oku, H., Hashimoto, K. & Ishikawa, M. Variable-focus lens with 1-kHz bandwidth. *Opt. Express* **12**, 2138–2149 (2004).
- Qi, B. *et al.* Dynamic focus control in high-speed optical coherence tomography based on a microelectromechanical mirror. *Opt. Comm.* **232**, 123–128 (2004).

19. Reddy, G.D. & Saggau, P. Fast three-dimensional laser scanning scheme using acousto-optic deflectors. *J. Biomed. Opt.* **10**, 064038 (2005).
20. Kleinfeld, D., Mitra, P.P., Helmchen, F. & Denk, W. Fluctuations and stimulus-induced changes in blood flow observed in individual capillaries in layers 2 through 4 of rat neocortex. *Proc. Natl. Acad. Sci. USA* **95**, 15741–15746 (1998).
21. Oheim, M., Beaurepaire, E., Chaigneau, E., Mertz, J. & Charpak, S. Two-photon microscopy in brain tissue: parameters influencing the imaging depth. *J. Neurosci. Methods* **111**, 29–37 (2001).
22. Mao, B.Q., Hamzei-Sichani, F., Aronov, D., Froemke, R.C. & Yuste, R. Dynamics of spontaneous activity in neocortical slices. *Neuron* **32**, 883–898 (2001).
23. Cossart, R., Ikegaya, Y. & Yuste, R. Calcium imaging of cortical networks dynamics. *Cell Calcium* **37**, 451–457 (2005).
24. Sasaki, T., Kimura, R., Tsukamoto, M., Matsuki, N. & Ikegaya, Y. Integrative spike dynamics of rat CA1 neurons: a multineuronal imaging study. *J. Physiol. (Lond.)* **574**, 195–208 (2006).
25. Salome, R. *et al.* Ultrafast random-access scanning in two-photon microscopy using acousto-optic deflectors. *J. Neurosci. Methods* **154**, 161–174 (2006).
26. Iyer, V., Hoogland, T.M. & Saggau, P. Fast functional imaging of single neurons using random-access multiphoton (RAMP) microscopy. *J. Neurophysiol.* **95**, 535–545 (2006).
27. Kurtz, R., Fricke, M., Kalb, J., Tinnefeld, P. & Sauer, M. Application of multiline two-photon microscopy to functional *in vivo* imaging. *J. Neurosci. Methods* **151**, 276–286 (2006).
28. Wang, X. *et al.* Astrocytic Ca<sup>2+</sup> signaling evoked by sensory stimulation *in vivo*. *Nat. Neurosci.* **9**, 816–823 (2006).
29. Feng, G. *et al.* Imaging neuronal subsets in transgenic mice expressing multiple spectral variants of GFP. *Neuron* **28**, 41–51 (2000).
30. Miesenböck, G. & Kevrekidis, I.G. Optical imaging and control of genetically designated neurons in functioning circuits. *Annu. Rev. Neurosci.* **28**, 533–563 (2005).